Biomaterials 99 (2016) 82–94

Contents lists available at ScienceDirect

Biomaterials

journal homepage: www.elsevier.com/locate/biomaterials

Substrate stiffness and matrix composition coordinately control the differentiation of liver progenitor cells

Andreas P. Kourouklis [1], Kerim B. Kaylan [1], Gregory H. Underhill*

Department of Bioengineering, University of Illinois at Urbana-Champaign, Urbana, IL 61801, United States

ARTICLE INFO

Article history:
Received 25 January 2016
Received in revised form
30 April 2016
Accepted 11 May 2016
Available online 12 May 2016

Keywords:
Extracellular matrix
Cellular microarrays
Traction force microscopy
Substrate stiffness
Liver progenitor cells

ABSTRACT

Recent approaches have utilized microfabricated platforms to examine combinations of microenvironmental signals that regulate stem and progenitor cell differentiation. However, the majority of these efforts have focused on the biochemical properties of extracellular matrix (ECM) or soluble factors without simultaneously exploring the biomechanical effects of cell–substrate interactions. To address this need, we combined a high-throughput approach for the analysis of combinatorial ECM cues with substrates of modular stiffness and traction force microscopy. This integrated approach enabled the characterization of cell-generated traction stress and phenotypic expression in response to ECM cues. We investigated the impact of substrate stiffness and ECM composition on the differentiation of bipotential mouse embryonic liver (BMEL) progenitor cells. We observed that hepatocyte differentiation was primarily regulated by ECM composition, and cholangiocyte differentiation was cooperatively influenced by ECM proteins and stiffness properties. In particular, stiffness-mediated cholangiocyte differentiation was observed for cells cultured on fibronectin, while collagen IV promoted differentiation independent of substrate stiffness. We demonstrated the influence of cell contractility and traction stress in early cholangiocyte specification and further uncovered the roles of ERK and ROCK in this differentiation process. Overall, these findings illustrate the involvement of biomechanical signals in liver progenitor differentiation. Further, this approach could enable investigations for a broad range of cell types and ECM proteins, providing an integrated platform for evaluating the combinatorial effects of biochemical and biophysical signals in cell differentiation.

1. Introduction

Liver progenitor cells are the bipotential precursors to hepatocytes, the functional parenchymal cells of the liver, and cholangiocytes, which form the bile duct epithelium. During development, these cells receive numerous signals from the microenvironment directing their differentiation towards either fate. For example, it is known that a gradient of TGFβ signaling localizes cholangiocyte differentiation to the periportal region [1,2]. Further activity by the Notch ligand JAG1 and receptor NOTCH2 is necessary for the formation of mature intrahepatic bile ducts [3–6]. Concurrently, interactions between β1-integrins and the extracellular matrix (ECM) proteins collagen I and laminin have been demonstrated to influence both cholangiocyte differentiation and morphogenesis [7–9]. We have recently studied the mechanisms by which progenitor differentiation is simultaneously regulated by these pathways, illustrating cooperative interactions between the TGFβ and Notch pathways, which are further influenced by ECM proteins [10]. While the importance of these biochemical signals in liver progenitor cell fate decisions has been investigated in detail, the role of mechanical cues is considerably less defined for this cell type.

Recent studies have demonstrated the implications of ECM stiffness in liver pathology (e.g., cirrhosis) [11–13] and further highlight the causative rather than the consequential role of ECM stiffness in the development of the fibrotic disease [14]. In other tissue contexts, mechanical signals and associated mechanotransduction have been broadly implicated in the regulation of stem and progenitor cell differentiation [15–17]. Studies of mesenchymal stem cell differentiation in particular have yielded a wealth of approaches for elucidating fundamental mechanobiology [18–20], including protein patterning [21–24],

* Corresponding author.
E-mail address: gunderhi@illinois.edu (G.H. Underhill).
[1] Contributed equally to this work.

http://dx.doi.org/10.1016/j.biomaterials.2016.05.016
0142-9612/

modular elastic substrates [25,26], and mechanical and biochemical gradient generation [27–30]. Despite the important information provided by these efforts, the complexity and less defined nature of the hepatic microenvironment requires the development of approaches to efficiently examine large sets of combinatorial ECM signals while maintaining select features of *in vivo* mechanobiology. Previous studies aimed at deconstructing combinatorial effects have exploited the fabrication of cellular microarrays of ECM proteins on elastic substrates [31–34]. In contrast with the demonstrated ability of cell microarrays to examine the effects of combinatorial biochemical signaling by ECM proteins, there have only been limited efforts to simultaneously investigate the role of the associated biophysical signals.

Fundamental investigations into cell mechanotransduction mechanisms have highlighted the critical interaction between the mechanical microenvironment and cell traction force. Cell traction force is generated through a myosin-dependent contractile mechanism in response to the adhesion of membrane receptors on ECM ligands and the subsequent activation of intracellular pathways [20]. The magnitude of the generated stress is regularly correlated with the assembly of intracellular structures [35] and subsequent signaling pathway activation plays an important role in several biological functions such as migration [36] and differentiation [37]. One of the most common methods for measuring traction force at the cell–ECM interface is the technique termed traction force microscopy (TFM) [38–41]. However, there have not been previous demonstrations of using TFM or other methods of traction measurement with cellular microarrays.

In this report, we demonstrate an approach for the integration of cell microarrays with substrates of modular mechanical characteristics and TFM. We illustrate the unique capability of this strategy to support the systematic investigation of the combined effects of ECM composition and substrate stiffness on cell traction force and differentiation. Our studies reveal previously unidentified characteristics of liver progenitor differentiation which could have important implications in the understanding of liver morphogenesis and disease.

2. Materials and methods

2.1. Cell culture

We utilized BMEL 9A1 cells between passages 28 and 37. These cells were cultured as previously described [42]. Briefly, cells were seeded on tissue culture plastic coated with collagen I (0.5 mg/ml) and subsequently cultured under controlled environmental conditions (37 °C and 5% CO_2). Treatment with trypsin-EDTA (0.25% [v/v]) for ≤10 min was used to detach cells for subculturing. Basal media for expansion consisted of RPMI 1640 + GlutaMAX (Life Technologies, 61870-127) with fetal bovine serum (10% [v/v], FBS), penicillin/streptomycin (1% [v/v], P/S), human recombinant insulin (10 μg/ml, Life Technologies, 12585-014), IGF-2 (30 ng/ml, PeproTech, 100-12), and EGF (50 ng/ml, PeproTech, AF-100-15). Differentiation media consisted of Advanced RPMI 1640 (Life Technologies, 12633-012) with FBS (2% [v/v]), P/S (0.5% [v/v]), L-glutamine (1% [v/v]), and minimum non-essential amino acids (1% [v/v], Life Technologies, 11140-050). During differentiation experiments, cells were seeded on arrays at ≥500E3 cells/slide for phenotypic assessment, 200E3 cells/dish in 35 mm glass-bottom Petri dishes for TFM, and 2.5E6 cells/slide for PA substrates conjugated with ECM using sulfo-SANPAH. Cells were allowed to adhere to ECM for at least 2 h before addition of experiment-specific treatments.

2.2. Growth factor and drug treatments

All growth factors and drugs were prepared and reconstituted according to the instructions of the manufacturers: TGFβ1 (R&D Systems, 240-B-002), 5 μg/ml in 4 mM HCl with 0.2% (w/v) bovine serum albumin; (−)-blebbistatin (Cayman Chemical, 13013), 1 mg/ml in dimethyl sulfoxide (DMSO); Y-27632 (Enzo Life Sciences, 270-333-M005), 5 mg/ml in deionized water (DiH_2O); NSC23766 (Tocris Biosciences, 2161), 10 mg/ml in DiH_2O; FR180204 (Sigma-Aldrich, SML0320), 10 mg/ml in DMSO; SP600125, 10 mg/ml in DMSO. For hepatocyte differentiation (TGFβ1-), cells were cultured in differentiation media for 72 h. For cholangiocyte differentiation (TGFβ1+), cells were cultured in differentiation media with TGFβ1 (1.5 ng/ml) for 24 h. Drugs were added to differentiation media at the following concentrations: (−)-blebbistatin, 25 μM; Y-27632, 10 μM; NSC23766, 10 μM; FR180204, 10 μM; SP600125, 10 μM.

2.3. Preparation of polyacrylamide hydrogels

Polyacrylamide (PA) hydrogels were prepared following previous protocols [31,43,44]. Briefly, 25 × 75 mm glass microscope slides were washed with 0.25% (v/v) Triton X-100 in DiH_2O and placed on an orbital shaker for 30 min. After rinsing with DiH_2O, slides were immersed in acetone and placed on the shaker for 30 min. The acetone wash was followed by immersion in methanol and another 30 min on the shaker. The slides were then washed with 0.05 N NaOH for 1 h, rinsed with DiH2O, air-dried, and placed on a hot plate at 110 °C until dry. For silanization, the cleaned slides were immersed in 2% (v/v) 3-(trimethoxysilyl)propyl methacrylate in ethanol and placed on the shaker for 30 min. The silanized slides were washed with ethanol on the shaker for 5 min, air-dried, and again placed on the hot plate at 110 °C until dry. For fabrication of hydrogels with specific elastic moduli, three prepolymer solutions with different acrylamide/bis-acrylamide percentage (w/v) ratios were prepared to achieve elastic moduli of 4 kPa (4% acrylamide, 0.4% bis-acrylamide), 13 kPa (6% acrylamide, 0.45% bis-acrylamide), and 30 kPa (8% acrylamide, 0.55% bis-acrylamide) and similar porosity [37]. Each of these prepolymer solutions were mixed with Irgacure 2959 (BASF, Corp.) solution (20% [w/v] in methanol) at a final volumetric ratio of 9:1 (prepolymer:Irgacure). This working solution was then deposited onto slides (100 μl/slide) and covered with 22 × 60 mm cover glasses. The sandwiched working solution was transferred to a UV oven and exposed to 365 nm UVA for 10 min (~240E3 μJ). After removing the cover glasses, the slides were immersed in DiH2O at room temperature for 3 d in order to remove excess reagents from the hydrogel substrates. Before microarray fabrication, hydrogel substrates were thoroughly dehydrated on a hot plate for ≥15 min at 50 °C.

2.4. Microarray fabrication

We fabricated microarrays as previously described [32,45,46]. Briefly, ECM proteins were mixed with an equal volume of 2 × ECM protein buffer (38% [v/v] glycerol in DiH_2O, 16.4 mg/ml sodium acetate, 3.72 mg/ml EDTA, 0.5% [v/v] Triton X-100, ~80 μl glacial acetic acid, pH = 4.8) and loaded into a 384-well V-bottom microplate. The final concentration of total ECM protein in each combination was 250 μg/ml; two-way combinations contained 125 μg/ml of each individual ECM protein. We utilized the following ECM proteins in our studies: collagen I (rat tail, EMD Millipore, 08-115), collagen III (human, EMD Millipore, CC054), collagen IV (human, EMD Millipore, CC076), fibronectin (human plasma, Sigma-Aldrich, F2006), and laminin (mouse, EMD Millipore, CC095). We additionally used 70 kDa dextran-rhodamine (2.5 mg/ml, Life Technologies, D-1841) as a marker for later array analysis. An

automated benchtop microarrayer (OmniGrid Micro, Digilab) was loaded with SMP3 Stealth microarray pins (ArrayIt) and used to transfer biomolecules from the 384-well microplate to the PA hydrogel substrate. This process produced arrayed domains approximately 150 μm in diameter. We stored fabricated arrays at room temperature and 65% RH overnight and then sterilized the next morning with 30 min UVC and immersion in 1 × phosphate buffered saline (PBS) supplemented with 1% (v/v) P/S. Cells were seeded on arrays immediately after sterilization per the section above.

2.5. Conjugation of ECM to PA hydrogels

We equilibrated sulfo-SANPAH (25 mg/ml in DMSO, G-Biosciences, 82022-840) to ambient temperature and immediately diluted to 1.04 mg/ml with 0.1 M HEPES buffer. We distributed 600 μl of this solution on PA substrates fabricated on 25 × 75 mm glass microscope slides (see above) and exposed substrates to UV light (300–460 nm) for 20 min. Substrates were subsequently washed with 0.1 M HEPES buffer for 5 min with agitation, after which we repeated the above steps twice more. After drying, we distributed 200 μl fibronectin (40 μg/ml in 0.1 M HEPES buffer) or 200 μl collagen IV (40 μg/ml in 0.1 M HEPES buffer) on each substrate and incubated at 4 °C overnight. We sterilized substrates with 30 min UV C in 1 × phosphate buffered saline (PBS) supplemented with 1% (v/v) P/S.

2.6. Traction force microscopy

For the TFM experiments, we adjusted our protocol in order to fabricate the PA hydrogels in glass-bottom 35 mm Petri dishes (Cell E&G, GBD00002-200) rather than on 25 × 75 mm microscope slides. This enabled us to perform TFM on live cells at 37 °C and 5% CO_2. To measure the cell-generated forces, we added 1 μm far-red fluorescent beads (Life Technologies, F-8816) to the 0.2% [v/v] working solution [41,47] and fabricated hydrogels with embedded beads by exposure to 365 nm UV A for 10 min.

We subsequently completed the hydrogel and array fabrication protocols as described above and seeded cells on the arrays. After completion of experiment-specific treatments, the arrays were transferred to an incubated (37 °C and 5% CO_2) Axiovert 200 M microscope (Carl Zeiss, Inc.). The microscope was used to capture phase contrast and far-red fluorescent micrographs to record cellular position and morphology along with bead displacement before and after treatment with sodium dodecyl sulfate (1% [v/v] in 1 × PBS). The captured images were analyzed in MATLAB using a previously-developed script to extract the traction stress and contractile moment [38,47]. All plots of traction stress and contractile moment show root mean square values.

2.7. Immunocytochemistry and imaging

Cells were treated with brefeldin A (10 μg/ml, R&D Systems, 1231/5) for 2 h and subsequently fixed in paraformaldehyde (4% [v/v] in 1 × PBS) for 15 min. Fixed samples were permeabilized with Triton X-100 (0.25% [v/v] in 1 × PBS) for 10 min and incubated in blocking buffer (5% [v/v] donkey serum in 1 × PBS) for 1 h at room temperature. We incubated samples for 1 h at room temperature with one or more of the following primary antibodies diluted in blocking buffer: mouse anti-ALB (1/50 from stock, R&D Systems, MAB 1455) and goat anti-OPN (1/60 from stock, R&D Systems, AF808). We next incubated samples for 1 h at room temperature with one or more of the following secondary antibodies diluted in blocking buffer: DyLight 550-conjugated donkey anti-mouse IgG (1/50 from stock, Abcam, ab98767) and DyLight 488-conjugated donkey anti-goat IgG (1/50 from stock, Abcam, ab96935). Samples were mounted in Fluoromount G with DAPI (Southern Biotech, 0100-20) and imaged the next day using an Axiovert 200 M microscope (Carl Zeiss, Inc.) and associated Zen Pro software. In order to capture entire arrays as one image for later analyses, we utilized the tiling feature of Zen Pro.

2.8. Immunoblotting

Cell lysates were collected using ice-cold RIPA lysis buffer (Thermo Scientific, 89900) with a protease inhibitor cocktail (Thermo Scientific, 78425) and phosphatase inhibitor cocktail (Thermo Scientific, 78428) per the manufacturer's instructions. Samples were immediately pulse sonicated 3 × 10 s and centrifuged at 14,000 × g for 15 min at 4 °C to remove cell debris. A BCA protein assay (Thermo Scientific, 23225) was performed in 96-well microplates per the manufacturer's instructions to determine total protein concentrations. Isodiluted samples were further diluted in 4 × Laemmli sample buffer and 2-mercaptoethanol (50 mM), denatured at 95 °C for 5 min, and loaded into a pre-cast 4–20% polyacrylamide gel (Bio-Rad, 567-1093) at 15 μg/well. Gels were run in 1 × tris/glycine/SDS at 200 V and 33–43 mA for 45 min. Transfer to 0.45 μm PVDF membranes (EMD Millipore, IPVH00010) occurred in 1 × tris/glycine and methanol (20% [v/v]) at 100 V using plate electrodes for 30 min, after which membranes were placed in a blocking solution of non-fat dry milk (5% [w/v]) in wash buffer (1 × tris-buffered saline and 0.05% [w/v] Tween-20) for 1 h with agitation. Membranes were subsequently incubated overnight on an orbital shaker at 4 °C with BSA (5% [w/v] in wash buffer) and rabbit anti-CK19 monoclonal antibody (1/10,000 from stock, Abcam, ab52625) or rabbit anti-phospho-ERK1/ERK2 (p44/42) (1/1000 from stock, Cell Signaling, 9101S). After 3 × 10 min rinses with wash buffer, the membrane was incubated for 1 h at room temperature with a solution of HRP-linked anti-rabbit IgG (1/3000 dilution from stock, Cell Signaling, 7074S) in wash buffer with non-fat dry milk (5% [w/v]). Membranes were subsequently rinsed 6 × 5 min with wash buffer, incubated for 5 min with chemiluminescent substrate (Thermo Scientific, 34080), and imaged (ChemiDoc XRS Imaging System, Bio-Rad). To confirm equal protein loading, membranes were treated with stripping buffer (Thermo Scientific, 21059) and labeled with monoclonal rabbit anti-β-actin (1/1000 from stock, Cell Signaling, 4970S) using the same protocol. Membranes labeled with anti-p-ERK were blocked and incubated with secondary in BSA (5% [w/v]) in wash buffer to prevent non-specific binding to phosphoproteins in non-fat milk. Protein content was quantified with NIH ImageJ [48].

2.9. Array analysis

Images of arrays were converted to individual 8-bit TIFF files per channel (e.g., red) by ImageJ and Fiji [48,49]. Image size was reduced to ≤100 MB by binning to reduce memory requirements during computational analysis. CellProfiler's IdentifyPrimaryObjects and IdentifySecondaryObjects modules were used to identify nuclei and immunolabeled regions, respectively [50]. The MeasureObjectIntensity module was used to quantify single-cell immunolabel intensity. The location of arrayed conditions within each image was automatically determined relative to manually-located dextran-rhodamine markers. In order to account for drift between experiments, quantile normalization was applied by biological replicate to the output of MeasureObjectIntensity. The percentage of cells positive for each marker was calculated by defining a cutoff 2 s.d. above the mean of a negative treatment.

2.10. Statistical analysis

Three biological replicates were performed for each experiment unless otherwise noted. For array studies, 4–6 slides (2 slides per biological replicate) totaling 40–60 islands/condition were analyzed unless otherwise noted. All data presented as mean ± s.e.m. We performed two-tailed, two-sample Student's *t*-tests with unequal variance for pairwise comparisons. Multiple regression analyses were performed in R using the base lm function. For each model, we confirmed homoscedasticity, normal distribution of residuals, and the absence of leveraged outliers using residual-fit, Q-Q, and scale-location plots. The unstandardized regression coefficient (β), which is reflective of the contrast (i.e., mean change) between two categorical variables, and associated P-value are provided for tests of specific hypotheses within a regression. For tests of overall regression significance, we evaluated the R^2 value, F-statistic, and P-value. For all hypothesis testing, $P < 0.05$ was considered significant.

3. Results

Our overall goal in these studies was to ascertain the collective impact of both substrate stiffness and ECM composition on liver cell fate decisions. To do so, we fabricated cellular microarrays on PA substrates of different elastic moduli (Fig. 1A) and subsequently cultured progenitor cells on the arrayed ECM combinations. At endpoint, we either assessed phenotypic marker expression (Fig. 1B) or performed TFM to measure traction stress (Fig. 1C). We were additionally able to assay response to chemical inhibition of intracellular signaling pathways in either format. In this work, we utilized bipotential mouse embryonic liver (BMEL) progenitor cells, which express markers of hepatocyte function when cultured at high-density or in aggregates [42]. BMEL cells are additionally capable of expressing cholangiocyte markers in Matrigel cultures or when treated with TGFβ1 [42,51,52], the latter of which we used in these studies to initiate cholangiocyte differentiation. For the cell microarray studies, we utilized albumin (ALB) and osteopontin

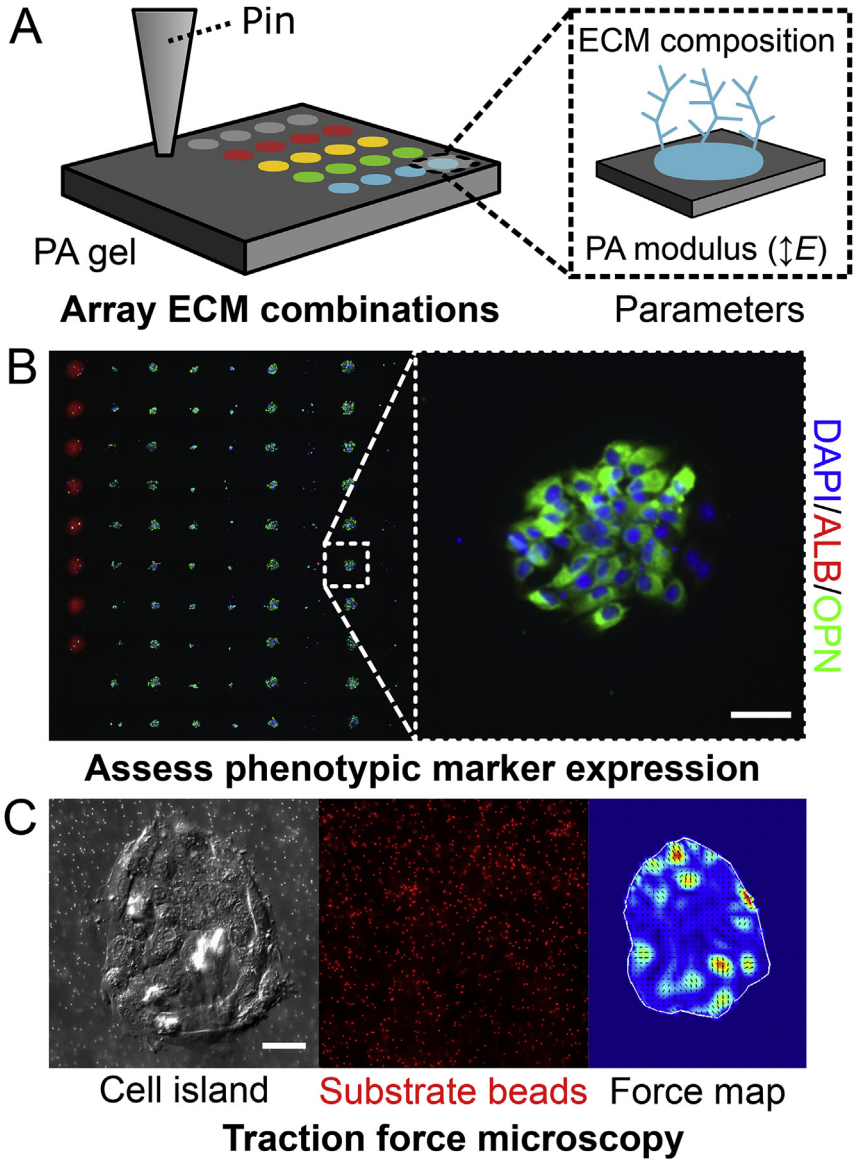

Fig. 1. An integrated platform for correlating fate processes with both biochemical and biophysical parameters. (A) ECM combinations were arrayed on a PA hydrogel substrate, enabling simultaneous control of ECM composition and PA modulus. (B) Cells cultured on ECM arrays were assessed for phenotypic marker expression. (C) Cells on PA substrates doped with fluorescent beads, enabling measurement of cell-generated forces on ECM arrays. Scale bars are 50 μm.

(OPN) as representative markers for hepatocyte and cholangiocyte differentiation, respectively. We have previously correlated expression of ALB with hepatocyte markers (*Hnf4a*, *Cebpa*) and OPN with cholangiocyte markers (*Sox9*, *Ggt1*) markers for BMEL cells within defined microenvironments [10].

3.1. Liver progenitor differentiation is influenced by both matrix composition and substrate stiffness

We characterized differentiation of BMEL progenitor cells on ECM-arrayed PA substrates of moduli 4 kPa, 13 kPa, and 30 kPa. We selected this range of stiffness for these studies as it has been previously demonstrated to be relevant for regulating the differentiation trajectories of stem cells in other tissue contexts [17]. Although normal liver tissue has been shown to exhibit stiffness near 150 Pa [53], the local stiffness near sites of progenitor differentiation within the developing liver has not been clearly determined. Further, alterations of stiffness within the 1–10 kPa range have been shown to influence the phenotypic characteristics of liver portal fibroblasts and mature cholangiocytes [54,55]. Arrays fabricated on these distinct substrates contained all two-factor combinations of collagen I (C1), collagen III (C3), collagen IV (C4), fibronectin (FN), and laminin (LN). After allowing cell adhesion for 2 h, we induced differentiation of cells on the ECM arrays towards the hepatocyte (low-serum differentiation medium) or cholangiocyte (low-serum differentiation medium with 1.5 ng/ml of TGFβ1) lineages and evaluated early (24 h and 72 h) upregulation of differentiation markers. Under hepatocyte induction conditions, cells exhibited an overall upregulation of ALB (Fig. 2A), with a number of the ECM compositions supporting percentages of ALB+ cells >40% at 72 h (Fig. 2B). Interestingly, the C4 condition, as well as 2-factor combinations containing C4, exhibited a substantial reduction in the percentage of ALB+ cells (Fig. 2B). Despite this reduction in ALB expression, cells cultured in the absence of TGFβ1 did not exhibit significant cholangiocyte differentiation regardless of ECM composition (Supplemental Fig. S1A). Regression analysis suggested a modest overall reduction in ALB+ cell percentage on 4 kPa versus 30 kPa (Supplemental Table S1), though many ECM conditions supported equal or slightly greater ALB+ cell percentages on 4 kPa substrates. However, during hepatocyte differentiation, total cell number was influenced by substrate stiffness, with cell number per ECM domain significantly reduced on the 4 kPa arrays across numerous ECM conditions (Supplemental Fig. S2). Collectively, these results suggest that, within the range tested, substrate stiffness does not exhibit a major effect on hepatocyte differentiation but may influence cell survival or adhesion during the differentiation process. Further, ECM composition, particularly the presence of C4, has a significant effect on hepatocyte

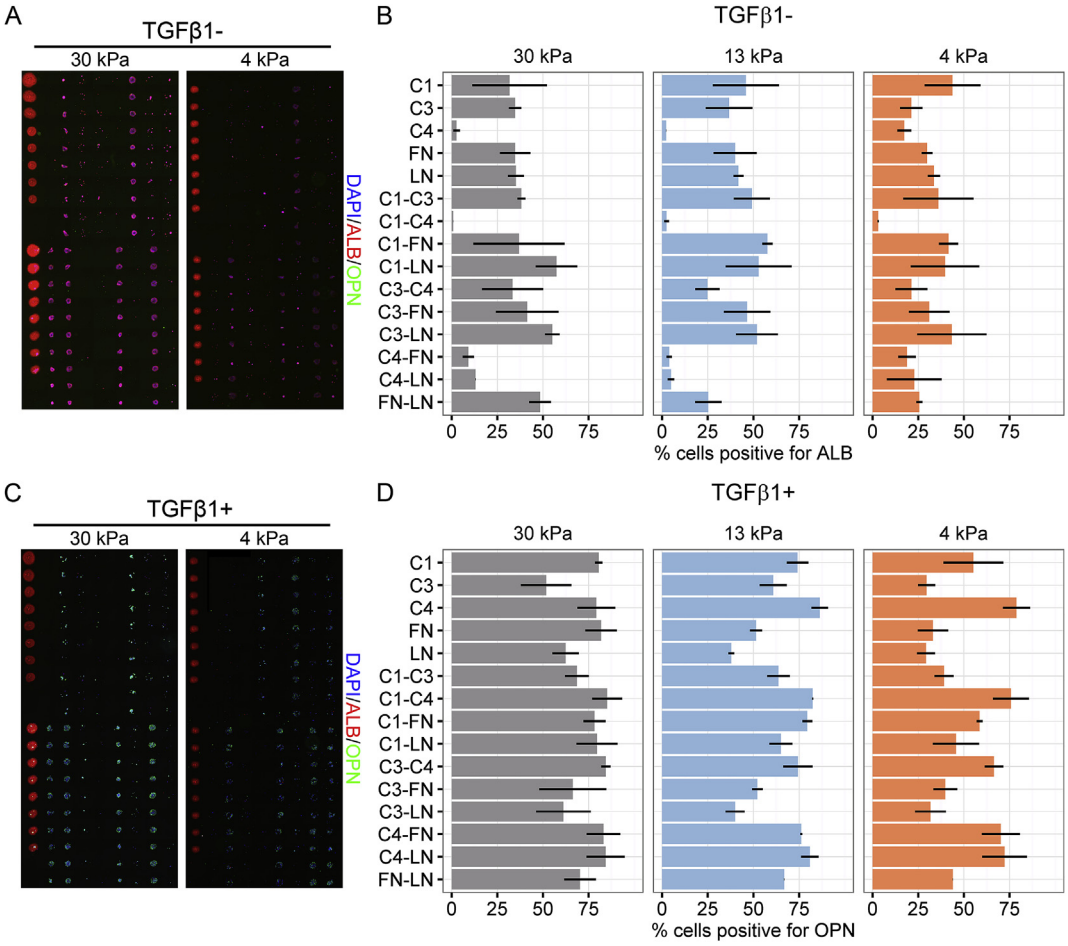

Fig. 2. Cell microarray-based analysis of the effects of ECM composition and substrate modulus on liver progenitor differentiation. (A) Representative arrays on 30 kPa and 4 kPa substrates after 72 h of differentiation without TGFβ1 labeled for nuclei (DAPI), ALB, and OPN. (B) Quantification of TGFβ1-arrays for ALB+ cell percentage. (C) Representative arrays on 30 kPa and 4 kPa substrates after 24 h of differentiation with TGFβ1 (1.5 ng/ml) labeled for nuclei (DAPI), ALB, and OPN. (D) Quantification of TGFβ1+ arrays for OPN+ cell percentage. Arrays in (A) and (C) are 4.5 × 9.0 mm (10 × 20 islands) and each island is ~150 μm in diameter. Data presented as mean ± s.e.m. with n = 2 and 40 total islands per condition. See also Supplemental Figs. S1 and S2 as well as Supplemental Tables S1 and S2.

differentiation of liver progenitor cells.

In parallel, we evaluated the effects of ECM and stiffness on cholangiocyte differentiation. We observed that 24 h of TGFβ1 treatment was sufficient to substantially upregulate OPN. Specifically, cells in these arrays were ALB- and OPN+ (Fig. 2C) and further demonstrated reduced percentages of OPN+ cells on 4 kPa substrates compared to 30 kPa on some ECM combinations (Fig. 2D). Regression analysis confirmed a significant reduction in OPN+ cell percentage on 4 kPa substrates ($\beta = -24.1\%$, $P < 0.001$) (Supplemental Table S1). The effect of ECM composition on OPN+ cell percentage between 30 kPa and 13 kPa substrates was less pronounced ($\beta = -8.88\%$, $P = 0.027$). Cells in arrays treated with TGFβ1 did not substantially express ALB regardless of ECM composition (Supplemental Fig. S1B). In order to ascertain the effects of individual ECM proteins, we performed separate regressions on data from the 30 kPa and 4 kPa substrates (Supplemental Table S2). Regression of the 30 kPa substrate data showed that different ECM combinations did not account for most variability in OPN+ cell percentage (adjusted $R^2 = 0.135$, $F_{[4,55]} = 3.30$, $P = 0.0170$). Regression of the 4 kPa substrate data, however, had a greater R^2 and was highly significant (adjusted $R^2 = 0.420$, $F_{[4,40]} = 8.97$, $P < 0.001$) and showed that combinations containing C4 had the greatest OPN+ cell percentage ($\beta = 40.8\%$, $P < 0.001$). Although not statistically significant, combinations containing C1 also had a greater OPN+ cell percentage ($\beta = 16.6\%$, $P = 0.129$) compared to other ECM proteins on 4 kPa substrates. C3, LN, and FN did not support differentiation as effectively as C4 and C1 on 4 kPa substrates. We selected C1, C4, FN, and all two-factor combinations therein for further analysis. Examination of OPN+ cell percentages for these ECM combinations from the TGFβ1+ arrays in Fig. 2 recapitulated the results of our regression analyses: In particular, C4 sustained cholangiocyte differentiation on 4 kPa substrates while FN does not (Fig. 3A). C1 exhibited an effect intermediate between C4 and FN. Fluorescent micrographs of the C1, C4, and FN arrayed conditions were consistent with these quantitative results (Fig. 3B).

Based on the cell microarray results, we scaled-up select conditions using chemical conjugation of individual ECM conditions to entire PA gel substrates and isolated bulk mRNA and protein for additional marker analysis. Following treatment with TGFβ1, cells cultured on C4 exhibited greater expression of CK19 compared to cells on FN (Fig. 3C and D). CK19 is a cholangiocyte marker shared with progenitor cells, and consistent with the OPN data, the most substantial difference between the effects of C4 and FN on CK19 expression was observed on 4 kPa substrates. In addition, we investigated the potential influence of ECM composition and stiffness on the expression of cell–cell and cell–matrix adhesion molecules. Notably, mRNA expression of E-cadherin (*Cdh1*), N-cadherin (*Cdh2*), and β1 integrin (*Itgb1*) was not significantly affected by substrate stiffness (Supplemental Fig. S3). ECM composition appeared to exhibit some influence, however, with the presence of FN leading to increased mRNA expression for N-cadherin and β1 integrin. Integrin αv exhibited a distinct mRNA expression profile with similar expression between C4 and FN conditions on 30 kPa substrates but relatively reduced expression on C4 compared to FN on 4 kPa substrates (Supplemental Fig. S3). Due to their previously recognized involvement in substrate stiffness sensing [56–58], we further examined mRNA expression of the kinases ROCK1 and RAC1. *Rock1* mRNA expression was relatively increased on C4 and FN 30 kPa substrates while *Rac1* mRNA expression was not influenced by composition or stiffness. In subsequent experiments (described below), we explored the functional role of these kinases in progenitor differentiation within the array format.

3.2. Cell contractility and traction stress in cholangiocyte differentiation

Cell contractility has been demonstrated to be a critical component of mechanotransduction pathways underlying cellular responses to substrate stiffness [20,58,59]. The selective reduction in cholangiocyte differentiation on soft substrates suggested the potential involvement of cell contractility in this differentiation process. To investigate this hypothesis, we treated cells with (−)-blebbistatin, an inhibitor of myosin II contractility, and observed a relative decrease in OPN+ cell percentage across each of the substrate stiffnesses (Fig. 4A). We did not observe significant changes in cell numbers resulting from (−)-blebbistatin treatment in these cholangiocyte differentiation arrays (Supplemental Fig. S4), indicating that the effect of blebbistatin on OPN

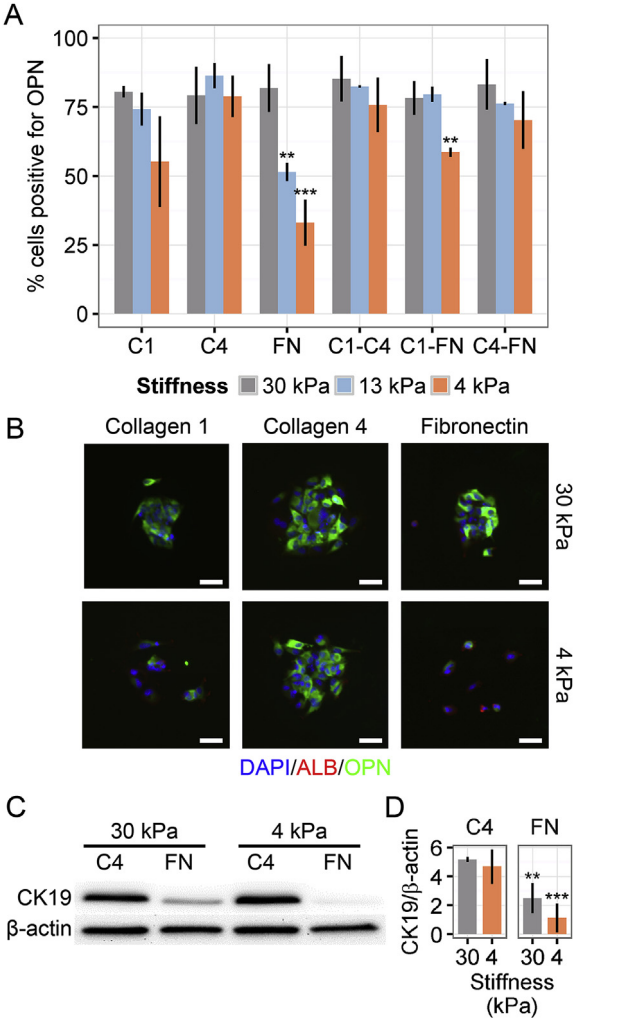

Fig. 3. Cholangiocyte differentiation is dependent on both ECM composition and substrate stiffness. (A) Selected ECM combinations from TGFβ1+ arrays highlighting differential response to stiffness between C4 and FN. Student's *t*-tests were performed against 30 kPa for each ECM combination. (B) Representative micrographs of the C1, C4, and FN arrayed conditions on 30 kPa and 4 kPa substrates labeled for nuclei (DAPI), ALB, and OPN. (C) Representative immunoblots of cells cultured for 24 h with TGFβ1 (1.5 ng/ml) on 30 kPa and 4 kPa substrates conjugated with C4 and FN using sulfo-SANPAH. (D) Quantification of CK19 immunoblot data normalized by β-actin. Student's *t*-tests were performed against 30 kPa C4 substrates. Data presented as mean ± s.e.m. with n = 2 and 40 total islands per condition in arrays and n = 3 for sulfo-SANPAH experiments. P-values indicated for $P < 0.05$ (*), $P < 0.01$ (**), and $P < 0.001$ (***). Scale bars are 50 μm. See also Supplemental Fig. S3.

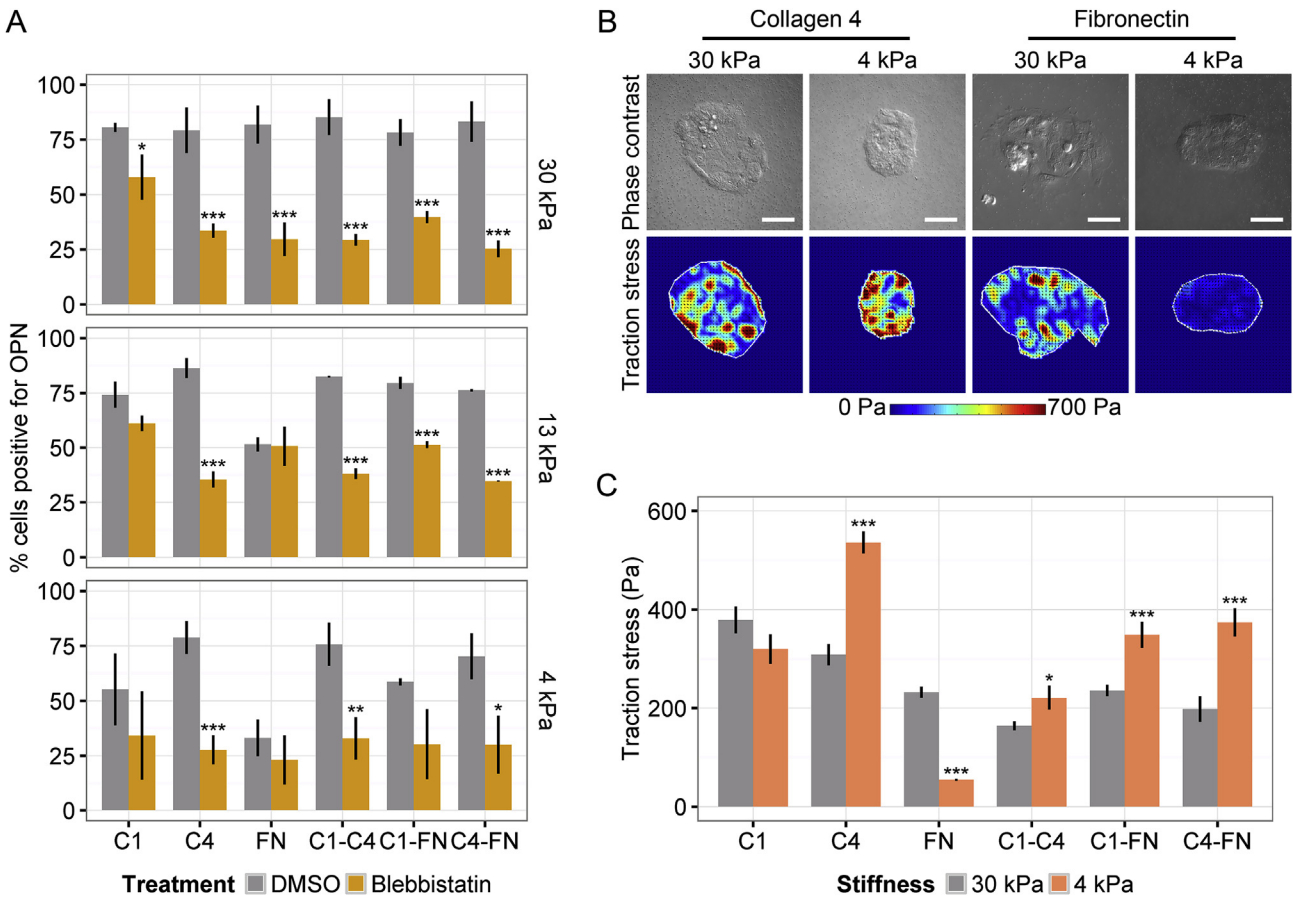

Fig. 4. Cell-generated traction stress integrates cues from both substrate stiffness and ECM composition. (A) Selected ECM combinations in TGFβ1+ arrays treated with DMSO (vehicle control) and (−)-blebbistatin (25 μM). Student's *t*-tests were performed against DMSO for each ECM combination on each stiffness. (B) Representative phase contrast micrographs and heat maps of traction stress for C4 and FN in TGFβ1+ arrays. (C) Quantification of root mean square values of traction stress in TGFβ1+ arrays. Student's *t*-tests were performed against 30 kPa for each ECM combination. Data presented as mean ± s.e.m. with n = 3 and 20–50 total islands per condition. P-values indicated for $P < 0.05$ (*), $P < 0.01$ (**), and $P < 0.001$ (***). Scale bars are 50 μm. See also Supplemental Figs. S4, S5, and S6.

expression was not due to an off-target effect on cell survival or proliferation. These results suggest that myosin II contractility is necessary for cholangiocyte differentiation independent of ECM composition and substrate stiffness.

We next sought to better understand the underlying biophysical mechanisms resulting in divergent cholangiocyte differentiation on C1, C4, and FN. We used TFM to examine both cell–substrate and cell–cell interactions during cholangiocyte differentiation in TGFβ1+ arrays. Specifically, we measured the traction stress, which is representative of interactions between the monolayer of BMEL cells on each arrayed ECM domain and the underlying PA hydrogel substrate. Interestingly, cell monolayers on C4 generated greater traction stress on 4 kPa substrates compared to 30 kPa ($P < 0.001$) (Fig. 4B and C). In contrast, the traction stresses on C1 and FN were reduced on 4 kPa substrates compared to 30 kPa. Only FN, however, demonstrated significant differences between the 4 kPa and 30 kPa substrates ($P < 0.001$) (Fig. 4C). Therefore, ECM composition determines the magnitude of cell-generated traction stress in response to substrate stiffness. In addition, cell monolayers on C1-C4 and C4-FN generated greater traction stress on 4 kPa substrates compared to 30 kPa. This result is in accordance with the effects of C4 on traction stress, indicating that C4 functionality supersedes that of C1 and FN alone. Unlike C1 and FN alone, C1-FN demonstrated greater traction stress on 4 kPa substrates compared to 30 kPa ($P < 0.001$).

As part of the traction force analyses, we further calculated the contractile moment, which has been previously utilized as a measure that reflects the strength of cell–cell interactions [47,60]. These measurements illustrate that the contractile moment declined on 4 kPa gels for all ECM proteins presented individually as well as the C1-C4 combination (Supplemental Fig. S5), and the most pronounced relative reduction was observed for the FN domains. Therefore, for these ECM conditions, reductions in substrate stiffness were correlated with reductions in the contractile moment. However, for cells on C1-FN and C4-FN, a different trend was observed, in which the distinct substrate stiffnesses did not influence contractile moment in a statistically significant manner.

Our TFM results indicate that within the context of cholangiocyte differentiation conditions (TGFβ1+), C4 supports cell traction stress on both 30 kPa and 4 kPa substrates. This effect was different than what we observed on FN, which exhibited dependence on the stiffness of the substrate. As a comparison, we additionally investigated cell traction stress on both C4 and FN in hepatocyte differentiation conditions (TGFβ1-) (Supplemental Fig. S6). In contrast to the results observed for cholangiocyte differentiation, traction stress was similarly reduced on 4 kPa versus 30 kPa substrates for both C4 and FN. These data suggest that the dependence of cell traction stress on ECM composition or stiffness is further regulated by the differentiation conditions, namely the presence of TGFβ1.

3.3. Effects of signaling pathway inhibitors on differentiation and cell traction stress

We next aimed to explore the mechanisms by which ECM characteristics and cell traction stress regulate cholangiocyte differentiation of progenitor cells. Within the microarray format, we induced cholangiocyte differentiation (TGFβ1+) and further treated the microarrays with a panel of signaling inhibitors or vehicle control (DMSO). Specifically, among the factors tested were inhibitors against extracellular-signal-regulated kinase (ERK), which modulates mitogen-activated protein kinase (MAPK) signaling through ECM–integrin interactions [61,62], and Rho-associated protein kinase (ROCK), which can increase myosin II activity by phosphorylation [63]. Treatment with an inhibitor of ERK (FR180204) reduced OPN+ cell percentages for all ECM combinations on 30 kPa substrates (Fig. 5A and B). Regression analysis confirmed that FR180204 reduced OPN+ cell percentages on 30 kPa ($\beta = -29.5\%$, $P < 0.001$) but not 4 kPa substrates ($\beta = -4.78\%$, $P = 0.354$) (Supplemental Table S3). In contrast, treatment with an inhibitor of ROCK (Y-27632) increased OPN+ cell percentages (Fig. 5A and B). These results were corroborated by regression analysis, which indicated increases in OPN+ cell percentage on both 30 kPa ($\beta = 16.3\%$, $P < 0.001$) and 4 kPa ($\beta = 26.8\%$, $P < 0.001$) substrates for treatment with Y-27632 (Supplemental Table S3).

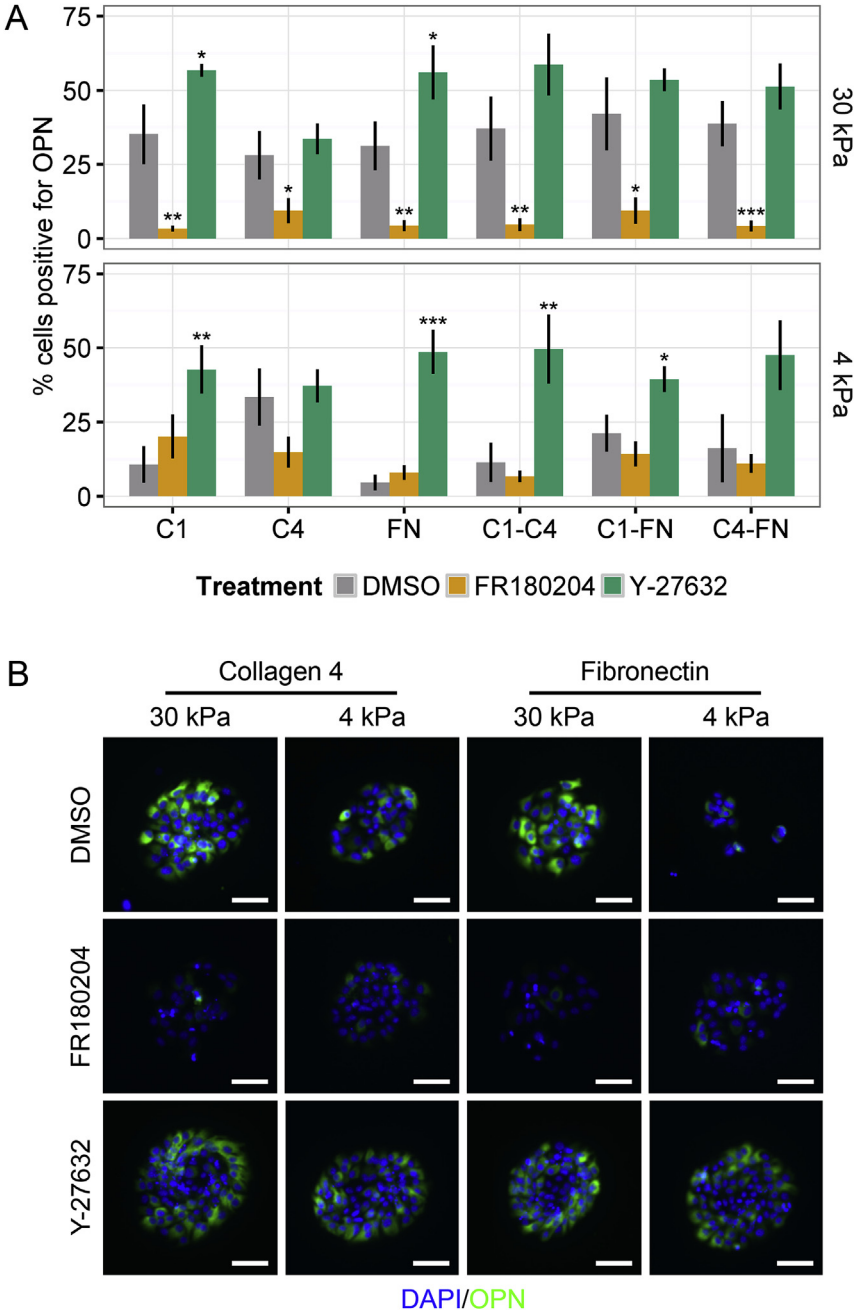

Fig. 5. Treatment of cell microarrays with signaling pathway inhibitors. (A) Quantification of OPN+ cell percentage on selected ECM combinations in TGFβ1+ arrays treated with inhibitors against ERK (FR180204, 10 μM) and ROCK (Y-27632, 10 μM). Student's *t*-tests were performed against DMSO for each treatment within each ECM combination. (B) Representative fluorescent micrographs of C4 and FN conditions labeled for nuclei (DAPI) and OPN. Data presented as mean ± s.e.m. with n = 3 and 60 total islands per condition. P-values indicated for $P < 0.05$ (*), $P < 0.01$ (**), and $P < 0.001$ (***). Scale bars are 50 μm. See also Supplemental Figs. S7 and S8 and Supplemental Table S3.

Notably, we observed statistically significant increases in OPN+ cell percentage for C1 and FN but not C4 on both 30 kPa and 4 kPa substrates (Fig. 5A).

Additionally, we used inhibitors against RAC1, a Rho family GTPase, and c-Jun N-terminal kinase (JNK) (Supplemental Fig. S7). RAC1 frequently opposes ROCK-mediated actin-myosin contractility [64,65] while JNK transduces integrin-mediated MAPK signaling, like ERK [66,67]. Treatment with an inhibitor of RAC1 (NSC23766) increased OPN+ cell percentages on 4 kPa substrates ($\beta = 38.9\%$, $P < 0.001$) but not 30 kPa substrates ($\beta = 5.37\%$, $P = 0.265$) (Supplemental Table S3). Treatment with an inhibitor of JNK (SP600125) increased OPN+ cell percentages on 4 kPa substrates ($\beta = 12.8\%$, $P = 0.0265$) but decreased them on 30 kPa substrates ($\beta = -10.7\%$, $P = 0.0275$) (Supplemental Table S3). We did not observe toxicity due to any of the drug treatments and observed comparable, if not greater, cells/island for the drug treatments in comparison to the DMSO control (Supplemental Fig. S8).

Due to the intriguing increase in cholangiocyte differentiation following ROCK inhibition, particularly on 4 kPa substrates, we hypothesized that ROCK inhibition would alter cell traction stress. Thus, we examined cell-generated contractility and traction stress using TFM within the cell microarray together with pharmacological inhibition of ROCK by Y-27632 (Fig. 6). We found ROCK inhibition reduced traction stress on both 4 kPa and 30 kPa substrates for all ECM combinations except FN (Fig. 6A and C). For 30 kPa substrates with FN, Y-27632 treatment was statistically indistinguishable from the DMSO control. For 4 kPa substrates with FN, however, the traction stress increased with Y-27632 treatment ($P < 0.001$). These characteristic effects are displayed in representative heat maps of the traction stress for C4 and FN on both 30 kPa (Fig. 6B) and 4 kPa (Fig. 6D) substrates. In addition, we calculated the contractile moment and observed decreases for 30 kPa substrates with Y-27632 treatment for all ECM combinations, including FN (Supplemental Fig. S9A). For 4 kPa substrates, the contractile moment decreased with Y-27632 treatment for C1, C4, and C1-FN and increased for FN and C4-FN (Supplemental Fig. S9B).

Based on our finding that ERK inhibition significantly reduced cholangiocyte differentiation within the arrays, we further investigated the role of ERK in the differentiation process. Using scaled-up substrates containing chemically conjugated C4 or FN, we examined the activation of ERK signaling through the immunoblot assessment of phosphorylated ERK1 and ERK2 (p-ERK). Following induction of cholangiocyte differentiation (TGFβ1+), p-ERK levels were slightly increased at 24 h relative to basal levels exhibited by undifferentiated BMEL cells (Fig. 7A and C), and then decreased relative to basal at 72 h (Fig. 7B and C). This increase at 24 h was observed for C4 on both 30 kPa and 4 kPa substrates. For the FN conditions, cells on 4 kPa substrates exhibited a modest reduction in p-ERK levels compared to cells on 30 kPa at the 24 h time point. These data are suggestive of a stiffness dependence of p-ERK activation on FN, a result consistent with the cholangiocyte

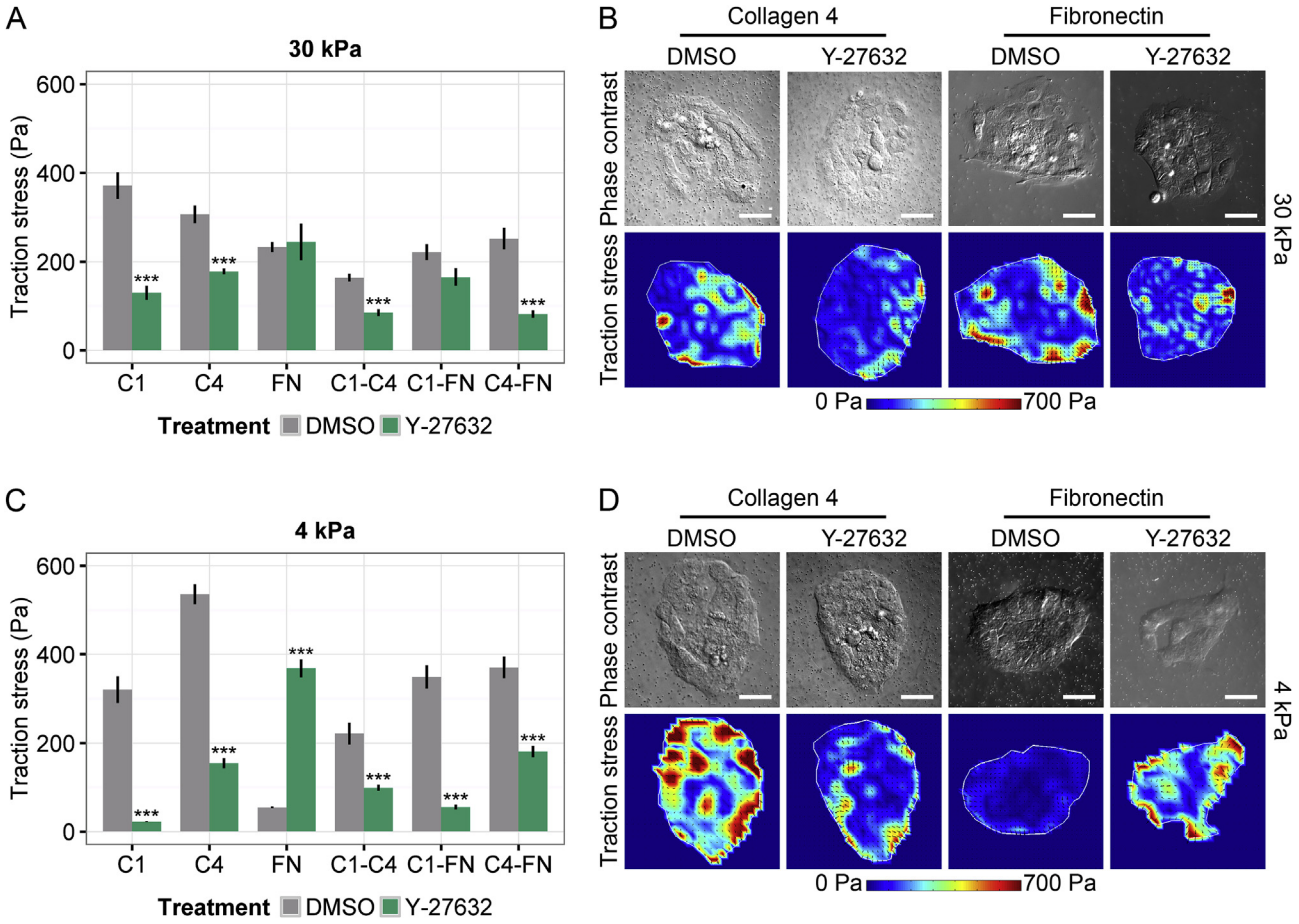

Fig. 6. Evaluation of cell traction stress in the context of ROCK inhibition. Traction stress generated in TGFβ1+ arrays on 30 kPa (A) and 4 kPa (C) substrates with DMSO (vehicle control) and an inhibitor of ROCK (Y-27623, 10 μM). Representative phase contrast micrographs and heat maps of traction stress for 30 kPa (B) and 4 kPa (D) substrates. Student's *t*-tests were performed against DMSO within each ECM combination. Data presented as mean ± s.e.m. with n = 3 and ~20 total islands per condition. P-values indicated for $P < 0.05$ (*), $P < 0.01$ (**), and $P < 0.001$ (***). See also Supplemental Fig. S9.

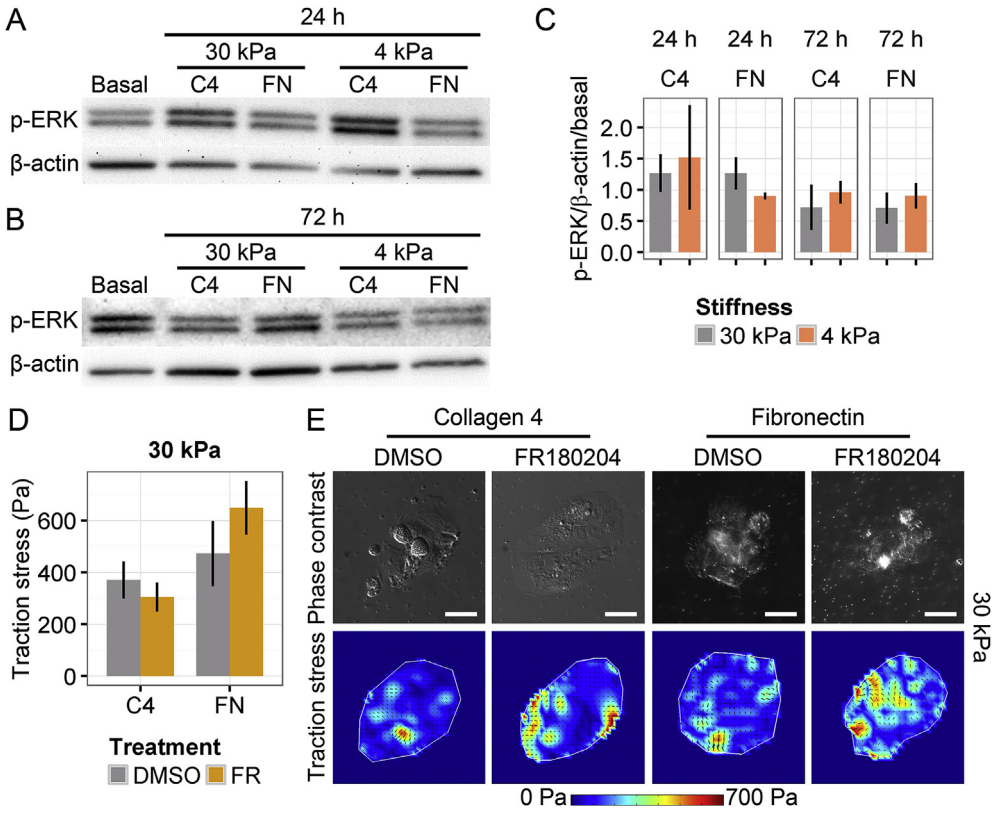

Fig. 7. Assessment of ERK signaling and effects on cell traction. Representative immunoblots for cells differentiated with TGFβ1 (1.5 ng/ml) for 24 h (A) and 72 h (B) on 30 kPa and 4 kPa substrates conjugated with C4 and FN using sulfo-SANPAH. (C) Quantification of p-ERK immunoblot data normalized by β-actin and basal controls. (D) Traction stress generated in TGFβ1+ arrays on 30 kPa substrates treated with DMSO (vehicle control) and an inhibitor of ERK (FR180204, 10 μM). (E) Representative phase contrast micrographs and heat maps of traction stress for C4 and FN. Data presented as mean ± s.e.m. with n = 3 and 20–25 total islands per condition in arrays. Scale bars are 50 μm.

differentiation for that ECM condition. In addition, we further investigated the potential influence of ERK inhibition on cell traction stress. Utilizing cell microarrays on 30 kPa substrates, we performed TFM analysis and measured the effect of the ERK inhibitor (FR180204) on cell traction on domains containing both C4 and FN. Notably, at 24 h of cholangiocyte differentiation, ERK inhibition did not significantly alter cell traction stress on either of the ECM conditions (Fig. 7D and E), indicating that ERK signaling is not an upstream regulator of the observed cell traction at that time point. Taken together, these data suggest that ERK signaling is likely one of the mechanisms sensing ECM composition and stiffness in these cells and may act downstream of cell traction stress in the mechanoregulation of cholangiocyte differentiation.

4. Discussion

Stem cell differentiation is regulated by features of the local microenvironment such as mechanical feedback [25,68], protein composition [69], and soluble factor presentation [15,70]. Previous studies extensively investigated the effects of select ECM proteins on cellular responses but the complexity of the multi-component ECM [16] requires the development of new strategies to further unveil the role of ECM biomechanics in cellular functionality. Similarly, the stiffness of the liver microenvironment has been shown to play a regulatory role in the function of mature hepatocytes [12,53]. These biomechanical effects have been associated with the activation of specific signaling pathways (e.g., ERK) [71,72] and are correlated with growth factor presentation [73]. Although healthy liver consists of relatively soft tissue with stiffness measuring from 150 to 600 Pa [11,53], local stiffness has been shown to be greater near the periportal region [53], where cholangiocyte differentiation and bile duct morphogenesis occur during liver development. In addition, liver stiffness can substantially increase during liver fibrosis and cirrhosis to ≥20 kPa [74–76]. Such conditions result from chronic liver injury that is often associated with ductular reactions within the adult liver consisting of proliferative cells exhibiting progenitor markers [77,78]. This suggests that progenitor differentiation may occur within the context of stiffening microenvironments in disease settings. Collectively, despite the potential role of ECM stiffness in liver progenitor differentiation, there have not been extensive studies to analyze this subject.

To assess potential cooperative effects of the biochemical and biophysical properties of ECM, we integrated cell microarrays with PA hydrogels exhibiting a range of stiffness. Using this approach, we found that liver progenitor cells commit toward a cholangiocyte phenotype on higher stiffness substrates. However, the effects of substrate stiffness on cholangiocyte differentiation varied upon the type of ECM protein arrayed over the elastic substrates. We have schematically summarized these overall findings in Fig. 8. In particular, liver progenitor differentiation was sensitive to substrate stiffness on FN, likely due to force-dependent unfolding [79,80] that enhances α5β1 integrin-mediated adhesion through the presence of the synergy peptide (e.g., PHSRN) [81]. In contrast with FN, presentation of C4 blunted stiffness-mediated cholangiocyte differentiation. This could be due to the formation of a mechanically robust network of C4 [82] or the C4-induced activation of α1β1 integrin that has been previously shown to mitigate stiffness sensing [83,84]. Notably, hepatocyte differentiation was substantially less affected by stiffness. However, ECM composition did

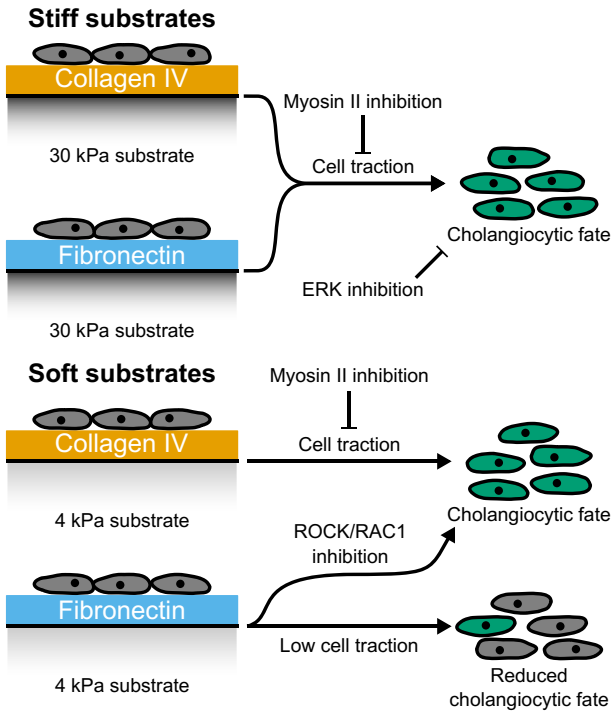

Fig. 8. Schematic summary of overall findings. Both C4 and FN support cholangiocyte differentiation of liver progenitors on stiff substrates while only C4 does so on soft substrates. Differentiation on stiff C4 and FN substrates is dependent on myosin II contractility and ERK signaling and is further associated with high traction stresses. In contrast, soft FN substrates are associated with low traction stress and result in reduced cholangiocyte differentiation. Inhibition of either ROCK or RAC1 increases cholangiocyte fate specification on soft FN substrates.

influence the expression of ALB, in particular, the presence of C4 reduced the expression of ALB relative to other ECM conditions. Together with the low expression of OPN on C4 under hepatocyte differentiation conditions, we hypothesize that the presence of C4 may maintain an undifferentiated progenitor phenotype, a mechanism that could be systematically explored in future studies utilizing the cell microarray platform. In addition, based on recent reports examining hepatocyte functionality [53], it is possible that hepatocyte differentiation of progenitor cells may be most significantly influenced by alterations in stiffness below 1 kPa. Future efforts could aim to adapt the microarray platform to support high-throughput investigations at this range of stiffness.

Our results demonstrate that the effects of different ECM proteins on cholangiocyte differentiation were consistent with the generated traction stress. Indeed, for FN and less profoundly for C1, cells generated significantly greater traction on stiffer substrates. In contrast, cells on C4 exhibited similar traction stress on both stiff and soft substrates. Therefore, the magnitude of traction stress connects ECM composition to the degree of cholangiocyte differentiation. Furthermore, actin-myosin contractility represents a critical cytoplasmic mechanism by which cells generate mechanical stress to sense and respond to their local microenvironment. In the cellular microarrays, inhibiting myosin II with (−)-blebbistatin diminished the effects of stiffness on cholangiocyte differentiation for every ECM composition, connecting actin-myosin contractility with cholangiocyte differentiation. Based on the TFM analysis, we also calculated a measure termed the contractile moment, which has been shown to be characteristic of the degree of intercellular traction at the cell–cell interface [47,60]. Interestingly, the contractile moment positively correlated with substrate stiffness for the presentation of individual proteins (e.g., C1, C4, or FN). In contrast, the presentation of ECM pairs supported stiffness-independent generation of traction stress and contractile moment. These results are suggestive of important interactions between cell–ECM and cell–cell signaling, which are further supported by the intriguing results observed following inhibition of ROCK and RAC1.

Since ROCK and RAC1 are known to promote cell contractility through myosin II phosphorylation and actin polymerization [85], respectively, we examined their contribution to cholangiocyte differentiation. Interestingly, inhibition of ROCK (and RAC1) substantially increased cholangiocyte differentiation on soft substrates. However, ROCK inhibition primarily reduced cell traction stress with a notable exception being FN, for which ROCK inhibition increased cell traction on 4 kPa substrates. Based on the previously demonstrated roles of ROCK and RAC1 in the destabilization of cell–cell adhesions within defined treatment contexts [65,86], we hypothesize that ROCK and RAC1 inhibition within the cell microarray format may enhance cell–cell interactions and therefore promote cholangiocyte differentiation in a manner that is not dependent on cell–ECM traction. Consequently, the treatment of progenitor cells with ROCK and RAC1 inhibitors facilitated cholangiocyte lineage specification independent of substrate stiffness. Building on our results presented here, the additional incorporation of techniques for directly measuring cell–cell traction forces, such as fluorescence resonance energy transfer (FRET)-based molecular tension sensors [87,88] into the array format could provide critical insights into potential cooperative interactions with intercellular adhesion signaling.

The ECM proteins presented in the cellular arrays (e.g., C1, C4 and FN) have been shown to support β1 integrin-mediated ERK signaling [89], whose phosphorylation has been previously correlated with stiffness-mediated differentiation in mature hepatocytes [90]. Here, the pharmacological inhibition of ERK significantly reduced cholangiocyte differentiation, particularly on stiff substrates. Furthermore, TFM showed that ERK inhibition had negligible effects on traction stress, suggesting that ERK activation is downstream of contractility. Moreover, the effects of stiffness on cholangiocyte differentiation coincided with the increased expression of phosphorylated ERK at 24 h which subsequently decreases by 72 h following differentiation induction. For FN, this increase in ERK phosphorylation was primarily observed on stiff substrates with the soft substrates exhibiting a level of phosphorylation below basal undifferentiated cells. In contrast, C4 presentation led to the highest observed levels of phosphorylated ERK at the 24 h time point. These characteristics of ERK activation are consistent with the stiffness effects on differentiation and traction stress identified for FN and C4. Collectively, these findings provide insight into the mechanisms that regulate cholangiocyte differentiation in response to combinatorial ECM cues. Despite the apparent roles of ERK and ROCK in the early stages of cholangiocyte specification, future experiments will be required in order to decouple their distinct contributions to liver progenitor differentiation.

5. Conclusions

We have examined how biomechanical cues and ECM proteins coordinately regulate the differentiation of liver progenitor cells. We combined cell microarrays on substrates of tunable stiffness with TFM in order to simultaneously assess phenotype and cell-generated traction stress. Cholangiocyte differentiation was dependent on both the type of ECM protein presented and the stiffness of the substrate. We showed that actin-myosin contractility controls cholangiocyte differentiation independent of ECM composition and stiffness. We further demonstrated the

involvement of ERK signaling in cholangiocyte differentiation though ERK inhibition did not directly affect traction stress generation. Overall, we have described an integrated approach to examine the mechanisms by which combinatorial biochemical and biomechanical ECM cues control cell fate. This strategy provides significant insight into the cell–ECM interactions during progenitor differentiation and can facilitate numerous future efforts examining the mechanisms underlying liver development and disease.

Disclosures

The authors indicate no potential conflicts of interest.

Acknowledgements

We gratefully acknowledge Hélène Strick-Marchand and Mary C. Weiss (Institut Pasteur) for providing BMEL cells. We also acknowledge Roberto A. Eguiluz and Deborah E. Leckband (University of Illinois at Urbana-Champaign) for advice and assistance with traction force microscopy, Ning Wang (University of Illinois at Urbana-Champaign) for providing the original traction force analysis script, and Austin Cyphersmith and Mayandi Sivaguru (University of Illinois at Urbana-Champaign) for assistance with microscopy. This work was supported by start-up funding from the University of Illinois at Urbana-Champaign.

Appendix A. Supplementary data

Supplementary data related to this article can be found at http://dx.doi.org/10.1016/j.biomaterials.2016.05.016.

References

[1] F. Clotman, et al., Control of liver cell fate decision by a gradient of TGF beta signaling modulated by Onecut transcription factors, Genes Dev. 19 (16) (2005) 1849–1854.
[2] F. Clotman, F.P. Lemaigre, Control of hepatic differentiation by activin/TGFbeta signaling, Cell Cycle 5 (2) (2006) 168–171.
[3] J.J. Hofmann, et al., Jagged1 in the portal vein mesenchyme regulates intrahepatic bile duct development: insights into Alagille syndrome, Development 137 (23) (2010) 4061–4072.
[4] P. Jeliazkova, et al., Canonical Notch2 signaling determines biliary cell fates of embryonic hepatoblasts and adult hepatocytes independent of Hes1, Hepatology 57 (6) (2013) 2469–2479.
[5] J.S. Tchorz, et al., Notch2 signaling promotes biliary epithelial cell fate specification and tubulogenesis during bile duct development in mice, Hepatology 50 (3) (2009) 871–879.
[6] Y. Zong, et al., Notch signaling controls liver development by regulating biliary differentiation, Development 136 (10) (2009) 1727–1739.
[7] N. Tanimizu, et al., alpha1- and alpha5-containing laminins regulate the development of bile ducts via beta1 integrin signals, J. Biol. Chem. 287 (34) (2012) 28586–28597.
[8] M. Yanai, et al., FGF signaling segregates biliary cell-lineage from chick hepatoblasts cooperatively with BMP4 and ECM components in vitro, Dev. Dyn. 237 (5) (2008) 1268–1283.
[9] N. Tanimizu, A. Miyajima, K.E. Mostov, Liver progenitor cells develop cholangiocyte-type epithelial polarity in three-dimensional culture, Mol. Biol. Cell 18 (4) (2007) 1472–1479.
[10] K.B. Kaylan, et al., Combinatorial microenvironmental regulation of liver progenitor differentiation by Notch ligands, TGFbeta, and extracellular matrix, Sci. Rep. 6 (23490) (2016).
[11] P.C. Georges, et al., Increased stiffness of the rat liver precedes matrix deposition: implications for fibrosis, Am. J. Physiol. Gastrointest. Liver Physiol. 293 (6) (2007) G1147–G1154.
[12] R.G. Wells, The role of matrix stiffness in regulating cell behavior, Hepatology 47 (4) (2008) 1394–1400.
[13] S.L. Friedman, Evolving challenges in hepatic fibrosis, Nat. Rev. Gastroenterol. Hepatol. 7 (8) (2010) 425–436.
[14] F. Kai, H. Laklai, V.M. Weaver, Force matters: biomechanical regulation of cell invasion and migration in disease, Trends Cell Biol. (2016), http://dx.doi.org/10.1016/j.tcb.2016.03.007, pii: S0962-8924(16)00050-7.
[15] D.E. Discher, D.J. Mooney, P.W. Zandstra, Growth factors, matrices, and forces combine and control stem cells, Science 324 (5935) (2009) 1673–1677.
[16] B. Trappmann, C.S. Chen, How cells sense extracellular matrix stiffness: a material's perspective, Curr. Opin. Biotechnol. 24 (5) (2013) 948–953.
[17] I.L. Ivanovska, et al., Stem cell mechanobiology: diverse lessons from bone marrow, Trends Cell Biol. 25 (9) (2015) 523–532.
[18] Kshitiz, et al., Control of stem cell fate and function by engineering physical microenvironments, Integr. Biol. Camb 4 (9) (2012) 1008–1018.
[19] L. MacQueen, Y. Sun, C.A. Simmons, Mesenchymal stem cell mechanobiology and emerging experimental platforms, J. R. Soc. Interface 10 (84) (2013) 20130179.
[20] V. Vogel, M. Sheetz, Local force and geometry sensing regulate cell functions, Nat. Rev. Mol. Cell Biol. 7 (4) (2006) 265–275.
[21] K.A. Kilian, et al., Geometric cues for directing the differentiation of mesenchymal stem cells, Proc. Natl. Acad. Sci. 107 (11) (2010) 4872.
[22] R.A. Desai, et al., Subcellular spatial segregation of integrin subtypes by patterned multicomponent surfaces, Integr. Biol. Camb 3 (5) (2011) 560–567.
[23] R. McBeath, et al., Cell shape, cytoskeletal tension, and RhoA regulate stem cell lineage commitment, Dev. Cell 6 (4) (2004) 483–495.
[24] G.C. Reilly, A.J. Engler, Intrinsic extracellular matrix properties regulate stem cell differentiation, J. Biomech. 43 (1) (2010) 55–62.
[25] A.J. Engler, et al., Matrix elasticity directs stem cell lineage specification, Cell 126 (4) (2006) 677–689.
[26] A. Engler, et al., Substrate compliance versus ligand density in cell on gel responses, Biophys. J. 86 (1 Pt 1) (2004) 617–628.
[27] M. Guvendiren, J.A. Burdick, Stiffening hydrogels to probe short- and long-term cellular responses to dynamic mechanics, Nat. Commun. 3 (2012) 792.
[28] J.R. Tse, A.J. Engler, Stiffness gradients mimicking in vivo tissue variation regulate mesenchymal stem cell fate, PLoS One 6 (1) (2011) e15978.
[29] W.R. Legant, et al., Microfabricated tissue gauges to measure and manipulate forces from 3D microtissues, Proc. Natl. Acad. Sci. U. S. A. 106 (25) (2009) 10097–10102.
[30] A.D. Rape, et al., A synthetic hydrogel for the high-throughput study of cell-ECM interactions, Nat. Commun. 6 (2015) 8129.
[31] N.E. Reticker-Flynn, et al., A combinatorial extracellular matrix platform identifies cell-extracellular matrix interactions that correlate with metastasis, Nat. Commun. 3 (2012) 1122.
[32] C.J. Flaim, S. Chien, S.N. Bhatia, An extracellular matrix microarray for probing cellular differentiation, Nat. Methods 2 (2) (2005) 119–125.
[33] C.J. Flaim, et al., Combinatorial signaling microenvironments for studying stem cell fate, Stem Cells Dev. 17 (1) (2008) 29–39.
[34] D.A. Brafman, et al., Investigating the role of the extracellular environment in modulating hepatic stellate cell biology with arrayed combinatorial microenvironments, Integr. Biol. Camb 1 (8–9) (2009) 513–524.
[35] N.Q. Balaban, et al., Force and focal adhesion assembly: a close relationship studied using elastic micropatterned substrates, Nat. Cell Biol. 3 (5) (2001) 466–472.
[36] X. Trepat, et al., Physical forces during collective cell migration, Nat. Phys. 5 (6) (2009) 426–430.
[37] J.H. Wen, et al., Interplay of matrix stiffness and protein tethering in stem cell differentiation, Nat. Mater 13 (10) (2014) 979–987.
[38] J.P. Butler, et al., Traction fields, moments, and strain energy that cells exert on their surroundings, Am. J. Physiol. Cell Physiol. 282 (3) (2002) C595–C605.
[39] R.W. Style, et al., Traction force microscopy in physics and biology, Soft Matter 10 (23) (2014) 4047–4055.
[40] X. Tang, et al., A novel cell traction force microscopy to study multi-cellular system, PLoS Comput. Biol. 10 (6) (2014) e1003631.
[41] J.H. Wang, J.S. Lin, Cell traction force and measurement methods, Biomech. Model Mechanobiol. 6 (6) (2007) 361–371.
[42] H. Strick-Marchand, M.C. Weiss, Inducible differentiation and morphogenesis of bipotential liver cell lines from wild-type mouse embryos, Hepatology 36 (4 Pt 1) (2002) 794–804.
[43] Y. Aratyn-Schaus, et al., Preparation of complaint matrices for quantifying cellular contraction, J. Vis. Exp. 46 (2010) e2173–e2173.
[44] J.R. Tse, A.J. Engler, Preparation of hydrogel substrates with tunable mechanical properties, Curr. Protoc. Cell Biol. (2010) 10.16.1–10.16.16.
[45] D.A. Brafman, S. Chien, K. Willert, Arrayed cellular microenvironments for identifying culture and differentiation conditions for stem, primary and rare cell populations, Nat. Protoc. 7 (4) (2012) 703–717.
[46] G.H. Underhill, C.J. Flaim, S.N. Bhatia, Extracellular matrix microarrays and stem cell fate, in: B. Parekkadan, M. Yarmush (Eds.), Methods in Bioengineering: Stem Cell Bioengineering, Artech House Publishers, Boston, MA, 2009, pp. 63–73.
[47] N. Wang, et al., Cell prestress. I. Stiffness and prestress are closely associated in adherent contractile cells, Am. J. Physiol. Cell Physiol. 282 (3) (2002) C606–C616.
[48] C.A. Schneider, W.S. Rasband, K.W. Eliceiri, NIH Image to ImageJ: 25 years of image analysis, Nat. Methods 9 (7) (2012) 671–675.
[49] J. Schindelin, et al., Fiji: an open-source platform for biological-image analysis, Nat. Methods 9 (7) (2012) 676–682.
[50] L. Kamentsky, et al., Improved structure, function and compatibility for CellProfiler: modular high-throughput image analysis software, Bioinformatics 27 (8) (2011) 1179–1180.
[51] H. Strick-Marchand, et al., Bipotential mouse embryonic liver stem cell lines contribute to liver regeneration and differentiate as bile ducts and hepatocytes, Proc. Natl. Acad. Sci. U. S. A. 101 (22) (2004) 8360–8365.
[52] A. Antoniou, et al., Intrahepatic bile ducts develop according to a new mode of tubulogenesis regulated by the transcription factor SOX9, Gastroenterology 136 (7) (2009) 2325–2333.

[53] S.S. Desai, et al., Physiological ranges of matrix rigidity modulate primary mouse hepatocyte function in Part Through hepatocyte nuclear factor 4 alpha, Hepatology (2016), http://dx.doi.org/10.1002/hep.28450.
[54] Z. Li, et al., Transforming growth factor-beta and substrate stiffness regulate portal fibroblast activation in culture, Hepatology 46 (4) (2007) 1246–1256.
[55] T. Komatsu, et al., Effect of extracellular matrix stiffness on ductular formation of biliary epithelial cells, in: 6th World Congress of Biomechanics (2010), 31, 2010, pp. 1095–1098.
[56] D. Riveline, et al., Focal contacts as mechanosensors: externally applied local mechanical force induces growth of focal contacts by an mDia1-dependent and ROCK-independent mechanism, J. Cell Biol. 153 (6) (2001) 1175–1185.
[57] K. Riento, A.J. Ridley, Rocks: multifunctional kinases in cell behaviour, Nat. Rev. Mol. Cell Biol. 4 (6) (2003) 446–456.
[58] D.E. Ingber, Cellular mechanotransduction: putting all the pieces together again, FASEB J. 20 (7) (2006) 811–827.
[59] M.A. Wozniak, C.S. Chen, Mechanotransduction in development: a growing role for contractility, Nat. Rev. Mol. Cell Biol. 10 (1) (2009) 34–43.
[60] R. Krishnan, et al., Substrate stiffening promotes endothelial monolayer disruption through enhanced physical forces, Am. J. Physiol. Cell Physiol. 300 (1) (2011) C146–C154.
[61] C.F. Lai, et al., Erk is essential for growth, differentiation, integrin expression, and cell function in human osteoblastic cells, J. Biol. Chem. 276 (17) (2001) 14443–14450.
[62] A.E. Aplin, et al., Integrin-mediated adhesion regulates ERK nuclear translocation and phosphorylation of Elk-1, J. Cell Biol. 153 (2) (2001) 273–282.
[63] M. Amano, et al., Phosphorylation and activation of myosin by Rho-associated kinase (Rho-kinase), J. Biol. Chem. 271 (34) (1996) 20246–20249.
[64] M. El-Sibai, et al., RhoA/ROCK-mediated switching between Cdc42- and Rac1-dependent protrusion in MTLn3 carcinoma cells, Exp. Cell Res. 314 (7) (2008) 1540–1552.
[65] E. Sahai, C.J. Marshall, ROCK and Dia have opposing effects on adherens junctions downstream of Rho, Nat. Cell Biol. 4 (6) (2002) 408–415.
[66] R.K. Barr, M.A. Bogoyevitch, The c-Jun N-terminal protein kinase family of mitogen-activated protein kinases (JNK MAPKs), Int. J. Biochem. Cell Biol. 33 (11) (2001) 1047–1063.
[67] G.L. Johnson, R. Lapadat, Mitogen-activated protein kinase pathways mediated by ERK, JNK, and p38 protein kinases, Science 298 (5600) (2002) 1911–1912.
[68] D.E. Discher, P. Janmey, Y.L. Wang, Tissue cells feel and respond to the stiffness of their substrate, Science 310 (5751) (2005) 1139–1143.
[69] C. Frantz, K.M. Stewart, V.M. Weaver, The extracellular matrix at a glance, J. Cell Sci. 123 (Pt 24) (2010) 4195–4200.
[70] J.S. Park, et al., The effect of matrix stiffness on the differentiation of mesenchymal stem cells in response to TGF-beta, Biomaterials 32 (16) (2011) 3921–3930.
[71] H. Rosenfeldt, F. Grinnell, Fibroblast quiescence and the disruption of ERK signaling in mechanically unloaded collagen matrices, J. Biol. Chem. 275 (5) (2000) 3088–3092.
[72] E.A. Klein, et al., Cell cycle control by physiological matrix elasticity and in vivo tissue stiffening, Curr. Biol. CB 19 (18) (2009) 1511–1518.
[73] Z. Li, et al., Transforming growth factor-β and substrate stiffness regulate portal fibroblast activation in culture, Hepatology 46 (4) (2007) 1246–1256.
[74] W.C. Yeh, et al., Elastic modulus measurements of human liver and correlation with pathology, Ultrasound Med. Biol. 28 (4) (2002) 467–474.
[75] S.K. Venkatesh, R.L. Ehman, Magnetic resonance elastography of liver, Magn. Reson Imaging Clin. N. Am. 22 (3) (2014) 433–446.
[76] M. Yin, et al., Assessment of hepatic fibrosis with magnetic resonance elastography, Clin. Gastroenterol. Hepatol. 5 (10) (2007), pp. 1207–1213.e2.
[77] T.A. Roskams, et al., Nomenclature of the finer branches of the biliary tree: canals, ductules, and ductular reactions in human livers, Hepatology 39 (6) (2004) 1739–1745.
[78] A.S. Gouw, A.D. Clouston, N.D. Theise, Ductular reactions in human liver: diversity at the interface, Hepatology 54 (5) (2011) 1853–1863.
[79] G. Baneyx, L. Baugh, V. Vogel, Fibronectin extension and unfolding within cell matrix fibrils controlled by cytoskeletal tension, Proc. Natl. Acad. Sci. U. S. A. 99 (8) (2002) 5139–5143.
[80] M.L. Smith, et al., Force-induced unfolding of fibronectin in the extracellular matrix of living cells, Plos Biol. 5 (10) (2007) 2243–2254.
[81] J.C. Friedland, M.H. Lee, D. Boettiger, Mechanically activated integrin switch controls alpha5beta1 function, Science 323 (5914) (2009) 642–644.
[82] P.D. Yurchenco, G.C. Ruben, Basement membrane structure in situ: evidence for lateral associations in the type IV collagen network, J. Cell Biol. 105 (6 Pt 1) (1987) 2559–2568.
[83] J.A. Eble, et al., The alpha-1-beta-1-integrin recognition site of the basement-membrane collagen molecule [Alpha-1(Iv)](2)Alpha-2(Iv), Embo J. 12 (12) (1993) 4795–4802.
[84] H. Louis, et al., Role of alpha1beta1-integrin in arterial stiffness and angiotensin-induced arterial wall hypertrophy in mice, Am. J. Physiol. Heart Circ. Physiol. 293 (4) (2007) p. H2597-604.
[85] S.T. Sit, E. Manser, Rho GTPases and their role in organizing the actin cytoskeleton, J. Cell Sci. 124 (Pt 5) (2011) 679–683.
[86] M.A. Frasa, et al., Armus is a Rac1 effector that inactivates Rab7 and regulates E-cadherin degradation, Curr. Biol. 20 (3) (2010) 198–208.
[87] N. Borghi, et al., E-cadherin is under constitutive actomyosin-generated tension that is increased at cell-cell contacts upon externally applied stretch, Proc. Natl. Acad. Sci. U. S. A. 109 (31) (2012) 12568–12573.
[88] T.J. Kim, et al., Dynamic visualization of alpha-catenin reveals rapid, reversible conformation switching between tension states, Curr. Biol. 25 (2) (2015) 218–224.
[89] F.G. Giancotti, Complexity and specificity of integrin signalling, Nat. Cell Biol. 2 (1) (2000) p. E13-4.
[90] J. Schrader, et al., Matrix stiffness modulates proliferation, chemotherapeutic response, and dormancy in hepatocellular carcinoma cells, Hepatology 53 (4) (2011) 1192–1205.